

Article

Enhanced Catalytic Dechlorination of 1,2-Dichlorobenzene Using Ni/Pd Bimetallic Nanoparticles Prepared by a Pulsed Laser Ablation in Liquid

Hyeon Jin Jung ^{1,†}, Seung Jun Lee ^{1,†}, Ravindranadh Koutavarapu ¹, Sung Kuk Kim ¹, Hyun Chul Choi ^{2,*} and Myong Yong Choi ^{1,*} 

¹ Department of Chemistry (BK21+) and Research Institute of Natural Science, Gyeongsang National University, Jinju 52828, Korea; lllsimple@gnu.ac.kr (H.J.J.); venus272@gnu.ac.kr (S.J.L.); ravindra.physicist@gmail.com (R.K.); sungkukkim@gnu.ac.kr (S.K.K.)

² Department of Chemistry, Chonnam National University, Gwangju 61186, Korea

* Correspondence: chc12@chonnam.ac.kr (H.C.C.); mychoi@gnu.ac.kr (M.Y.C.); Tel.: +82-55-772-1492 (M.Y.C.)

† These authors contributed equally to this work.

Received: 11 August 2018; Accepted: 7 September 2018; Published: 10 September 2018



Abstract: Bimetallic nanoparticles (NPs) exhibit advantageous electrical, optical, and catalytic properties. Among the various NP synthesis methods, pulsed laser ablation in liquid (PLAL) is currently attracting much attention because of its simplicity and versatility. In this study, a pulsed laser was used to produce nickel/palladium (Ni/Pd) bimetallic NPs in methanol and deionized water. The morphological and optical properties of the resulting Ni/Pd bimetallic NPs were characterized. The synthesized Ni/Pd bimetallic NPs were used for the dechlorination of 1,2-dichlorobenzene (1,2-DCB) under various conditions. The dechlorination rates of 1,2-DCB while using single (Ni and Pd) and bimetallic (Ni powder/Pd and Ni/Pd) NPs were investigated. The results showed that the Ni/Pd bimetallic NPs with 19.16 wt.% Pd exhibited much enhanced degradation efficiency for 1,2-DCB (100% degradation after 30 min). Accordingly, the results of enhanced the degradation of 1,2-DCB provide plausible mechanism insights into the catalytic reaction.

Keywords: Ni/Pd; bimetallic nanoparticles; pulsed laser ablation in liquid; 1,2-dichlorobenzene; dechlorination

1. Introduction

Global industrialization and the resulting continuous changes to environmental quality have caused serious water pollution problems. Chlorinated organic compounds (COCs), including alkyl and aryl chlorinated compounds, are widely used as raw materials, intermediates, and organic solvents in the chemical, agricultural and electronics industries [1,2]. However, COCs are toxic to humans and create health risks, such as birth defects, developmental impairment, infertile immune suppression, and cancer [3]. These COCs are environmentally persistent and they are challenging to directly degrade. Therefore, the decomposition of COCs in aqueous solutions and soil has received special research consideration [4]. Among the various COCs, 1,2-dichlorobenzenes (1,2-DCBs) are ubiquitously used and can be found in all major ecosystems [5]. Hence, there is a desperate need for efficient 1,2-DCB dechlorination methods that are suitable for treating both industrial wastewater and contaminated groundwater.

Many processes have been reported for the removal of 1,2-DCB, including advanced oxidation processes, photocatalytic reactions, ozonolysis, and catalytic ozonolysis [6]. Recently, catalytic

dechlorination of COCs at rates that are much faster than biodegradation have been reported. Moreover, catalytic reactions can be carried out at room temperature and atmospheric pressure [7]. Bimetallic nanoparticles (NPs) are of great scientific and technological interest [8], because they exhibit more improved electronic, optical, and catalytic properties than those of monometallic counterparts [9].

Thus far, precious metals, such as Pt, Pd, and Rh, and base metals, such as Co, Fe, and Ni, are the most commonly used metals for catalytic COC dechlorination in either liquid or gaseous environments [10–15]. Among these metals, Pd has exhibited the best performance in terms of activity and selectivity [16]. However, Pd is inactivated because of the formation of surface metal halides, and the loss of the active species. To improve the durability of Pd, a second metal can be incorporated to alter the surface geometric arrangement and the electronic properties of Pd [17,18]. Various bimetallic catalysts, such as Pd/Fe, Pd/Au, Pd/Pt, and Pd/Cu, have been reported. All of these bimetallic systems show improved catalytic performance when compared with their monometallic counterparts [19–22]. For example, Danish et al. demonstrated that natural zeolite-supported Fe/Cu bimetallic NPs had significantly improved the degradation of trichloroethylene than their monometallic nanostructured counterparts [23,24]. Mallikarjuna et al. showed that Cu/Pd bimetallic NPs had improved the catalytic hydrogenation performance of methyl orange, methylene blue, and 4-nitrophenol [25]. Zhao et al. designed Pd/Fe bimetallic NPs with enhanced 2,4-dichlorophenol dechlorination performance [26].

Reductive dechlorination is plausible by using a single oxidizing zero-valent metallic catalyst, like Ni^0 or Fe^0 , with direct electron transfer from the metal to the adsorbed substrate. Bimetallic catalysts can efficiently dechlorinate because two metals of potentially differing oxidation states can be employed. One metal should exist in the zero-valent form so as to have a negative reduction potential. This produces emerging hydrogen when it comes into contact with water through anodic oxidization. The other metal should have a relatively high positive reduction potential, such as Pd^{2+} or Ag^+ , to act as the hydrogenating catalyst. Moreover, this second metal converts the resulting hydrogen into a metal-hydride that can reduce the target substrate [27,28].

Numerous techniques have been employed for the synthesis of bimetallic NPs, including chemical precipitation, hydrothermal reduction, photo-deposition, and cathodic electro-deposition [29–32]. These techniques require complicated synthetic processes, high temperatures, organic reducing agents, and surfactants, and tend to fabricate aggregated NPs, which, however, decreased the catalytic activities. By contrast, pulsed laser ablation in liquid (PLAL) is an easy, efficient, and environmentally friendly method for synthesizing various nanocomposites. Thus, the PLAL generates various sizes and shapes of nanocomposites by controlling the PLAL conditions. Moreover, the well dispersed NPs produced by PLAL typically improve their catalytic activities [33].

In this study, Ni/Pd bimetallic NPs were synthesized for the first time via the PLAL of a Ni plate in a PdCl_2 solution. The optimum loading of Pd onto Ni NPs was successfully controlled to improve the dechlorination rates for 1,2-DCB treatment. X-ray diffraction (XRD), field-emission scanning electron microscopy (FE-SEM), high-resolution transmittance electron microscopy (HRTEM), and fast Fourier transform (FFT) analysis have been employed to characterize the prepared Ni/Pd bimetallic NPs.

2. Results and Discussion

2.1. Structural and Morphological Analysis

The XRD patterns of pure Ni and Ni/Pd bimetallic NPs (Pd concentration ratio of 1.60, 6.19, 19.16, and 24.29 wt.%) were measured, and it is shown in Figure 1. Figure 1a shows the diffraction peak of pure Ni NPs produced in methanol by the PLAL technique. The 2θ values corresponding to 43.98° , 51.29° , and 75.58° can be indexed to the (111), (200), and (220) planes of Ni (marked by #), respectively, to reveal a face-centered cubic (fcc) structure (JCPDS #01-087-0712) [34,35]. Figure 1b–e shows the XRD patterns of the Ni/Pd bimetallic NPs; as the concentration of Pd increases, the broad peaks with weak intensity (related to Pd) increases slightly. The intensity peaks at 40.06° , 46.16° , 68.29° , and 81.36°

correspond to the (111), (200), and (220) planes of fcc Pd NPs (marked by *) (JCPDS #01-088-2335), respectively [36]. No additional peaks were noticed in the XRD patterns, thus demonstrating the high purity of the as-prepared samples.

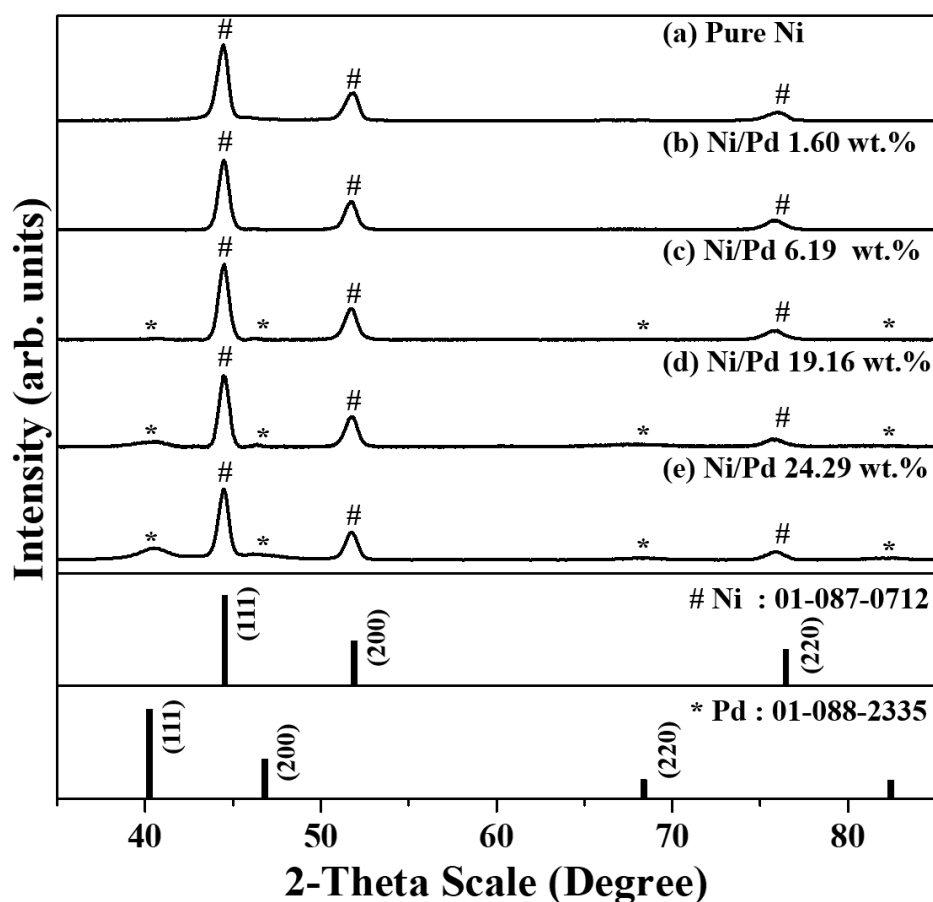


Figure 1. X-ray diffraction (XRD) patterns of (a) pure Ni and (b–e) Ni/Pd bimetallic nanoparticles (NPs) with different Pd loadings. The peaks marked by ‘#’ at 43.98°, 51.29°, and 75.58° are indexed to the (111), (200), and (220) planes of fcc structure Ni NPs (JCPDS #01-087-0712). The intensity peaks marked by ‘*’ at 40.06°, 46.16°, 68.29°, and 81.36° correspond to the (111), (200), and (220) planes of fcc Pd NPs (JCPDS #01-088-2335), respectively.

Figure 2a–d displays the HRTEM images of the Ni/Pd bimetallic NPs. About 5 nm Pd NPs were loaded onto the Ni NPs. The particles appear spherical in shape with a non-uniform size. Figure 2e shows the formation of Pd NPs on the surface of the Ni NPs. From the HRTEM images, the deposition of Pd NPs onto the spherical Ni surface gradually increases with respect to the Pd concentration, which confirms that Pd NPs adhere to the Ni NPs. Figure 2f,g display the inter-planar spacing of 0.206 and 0.222 nm attributed to Ni NPs in the (111) fcc plane [37] and the Pd NPs indexed to the (111) fcc plane [38], respectively. HRTEM mapping analysis was executed for the accurate identity and distribution of the Ni and Pd composition in the nanocomposites. Figure 2h displays the mapping image of Ni/Pd bimetallic NPs. The HRTEM mapping images for Ni (red) and Pd (green) are shown in Figure 2j,k, respectively. Through the mapping analysis, the Pd NPs were uniformly distributed onto the Ni NPs. Moreover, the elemental composition of the as-prepared sample used in this study (Ni, Pd) was determined while using EDS (Figure 2i). The EDS spectrum demonstrates the presence of Ni and Pd in the sample. In the spectrum, any impurities were detected, thus confirming the presence of prepared samples with the anticipated composition and high purity. The results are in good agreement with the XRD results (Figure 1). Additional information regarding the FE-SEM, HRTEM images, and selected area electron diffraction (SAED) characterization of pure Ni can be found in Figure S1.

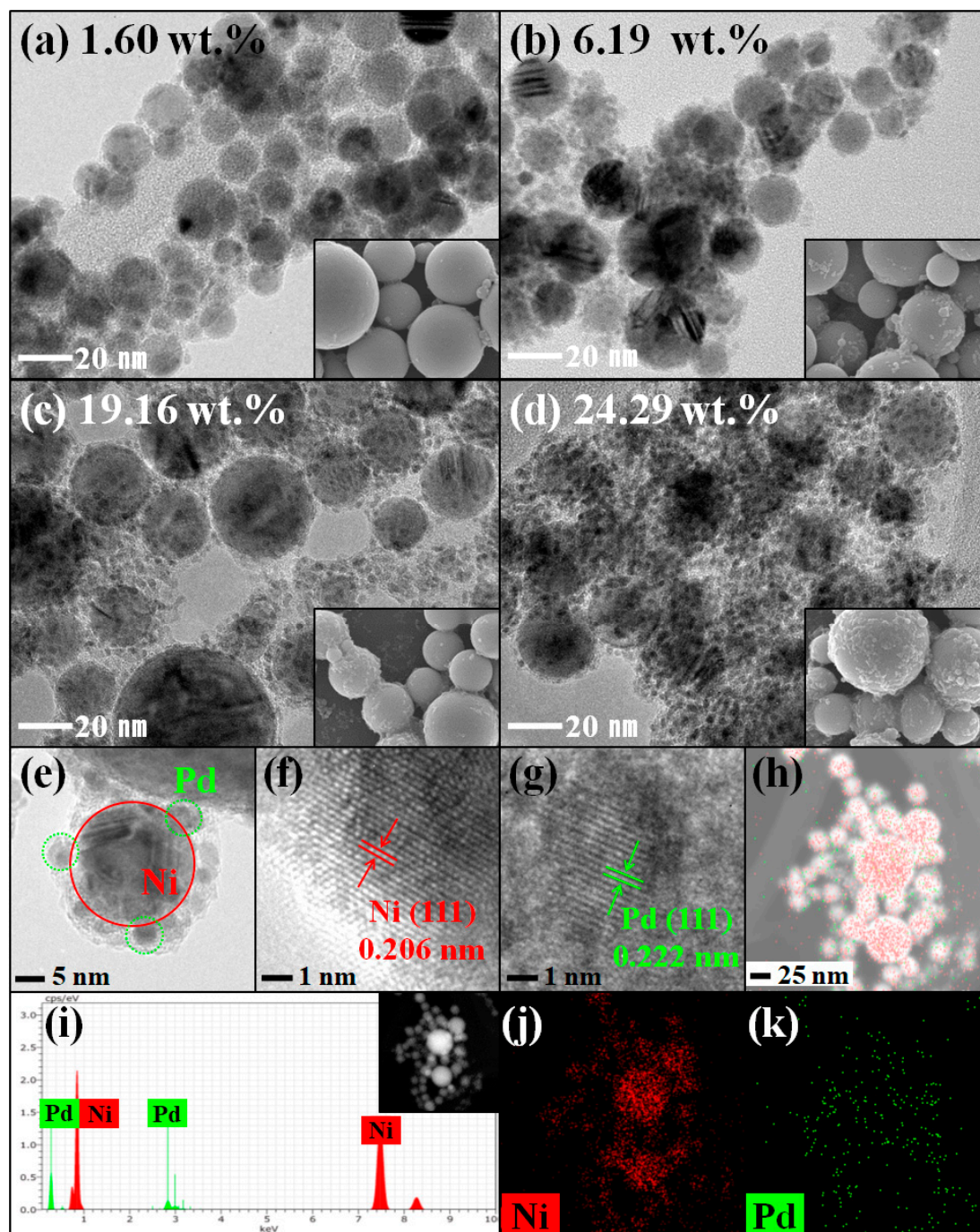


Figure 2. (a–d) High-resolution transmittance electron microscopy (HRTEM) images of Ni/Pd bimetallic NPs with various Pd loadings. (e) Pd NPs on the surface of Ni NPs. (f–k) selected area electron diffraction (SAED) and energy dispersive X-ray spectroscopy (EDS) patterns of Ni and Pd NPs.

2.2. Catalytic Dechlorination of 1,2-DCB Using Ni/Pd Bimetallic NPs

The dechlorination of 1,2-DCB, which is a typical environmental pollutant of soil and water sources, by using various NPs as catalysts was investigated. The 1,2-DCB dechlorination mechanism involves a substitution reaction of Cl to H on the Ni/Pd bimetallic NPs and it results in benzene as the final degradation product [39]. It is well known that Pd is a good hydrogen activation catalyst when H_2 is present [40]. Thus, the dechlorination efficiency was verified by changing the Pd amounts in the Ni NPs. Figure 3a displays the catalytic 1,2-DCB dechlorination as a function of Pd wt.% over 1 h. The dechlorination efficiency of 1,2-DCB was increased as the wt.% of Pd reached 19.16 wt.%.

However, a further increase in Pd loading decreased the dechlorination efficiency. The additional Pd NPs (24.29 wt.%) aggregated and minimized the surface energies, thus causing the change in morphology of the Pd NPs in the Ni/Pd system. This additional Pd doping has caused the reduced surface area of Pd and the decrease in the 1,2-DCB degradation rate [41].

To quantitatively determine the dechlorination efficiency of the Ni/Pd bimetallic NPs, the kinetic rate constants of the 1,2-DCB dechlorination reaction were calculated while using the pseudo-first-order correlation: $-\ln(C_t/C_0) = kt$, where C_t and C_0 are the concentration of 1,2-DCB at times t and 0 , respectively, and k is the reaction rate constant (min^{-1}). The plot of $\ln(C_t/C_0)$ as a function of reaction time for the dechlorination reaction of 1,2-DCB by various wt.% of Pd loading onto Ni NPs showed a linear correlation (Figure S2). The rate constants were determined as 0.049×10^{-4} , 0.0278 , 0.0990 , and 0.0607 min^{-1} for the sample of 1.60, 6.19, 19.16, and 24.29% Pd/Ni NPs, respectively. Among the as-synthesized Ni/Pd bimetallic NPs, 19.16% Pd/Ni NPs showed the highest catalytic efficiency.

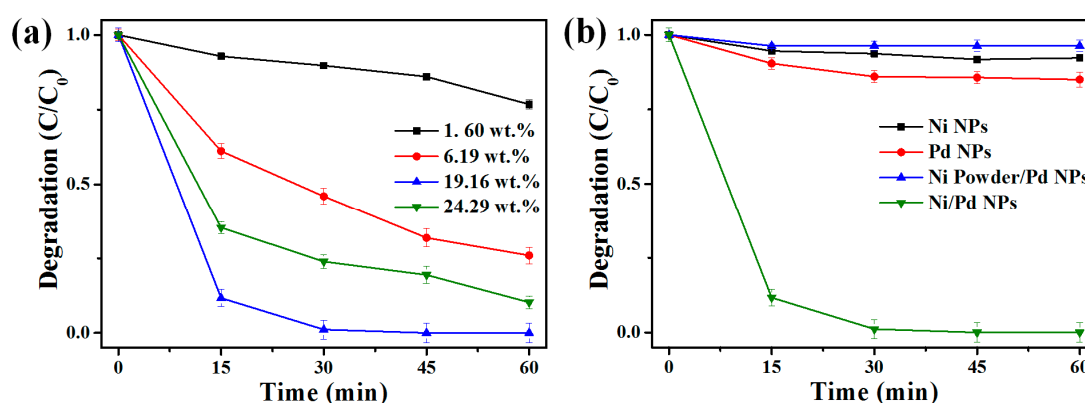
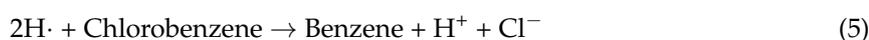
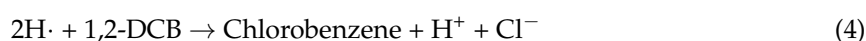


Figure 3. (a) Catalytic degradation of 1,2-DCB using Ni/Pd bimetallic NPs of various Pd loadings. (b) Catalytic degradation of 1,2-DCB for Ni, Pd, Ni powder/Pd NPs, and Ni/Pd bimetallic NPs.

Figure 3b shows the 1,2-DCB degradation rate comparison of the four different NPs fabricated in this study. The degradation rates of 1,2-DCB were very low in the case of monometallic Ni NPs, and it was a little better for the monometallic Pd NPs. These results clearly indicate that 1,2-DCB degradation while using monometallic Ni and Pd NPs requires 5 h [42]. For the case of bimetallic Ni powder/Pd NPs, the degradation efficiency was also low. However, the degradation efficiency was high for the Ni/Pd bimetallic NPs, reaching 100% 1,2-DCB degradation after 30 min. Furthermore, the degradation efficiency is much higher than those of the previously reported bimetallic NPs synthesized by other methods [43,44].

2.3. Mechanism of 1,2-DCB Degradation on the Ni/Pd Bimetallic NPs

The reductive 1,2-DCB degradation reaction in the Ni/Pd bimetallic catalytic system can be described, as follows:



In the case of Ni/Pd bimetallic NPs, as Ni is oxidized, protons from methanol are reduced to form molecular hydrogen at the Ni surface (Equations (1) and (2)). On the Ni/Pd bimetallic NPs surface, a galvanic cell process is involved [45], as shown in Figure 4. Ni and Pd act as anode and cathode, respectively, and the electrons that are transferred from Ni reduce the protons to form highly

active atomic hydrogen radicals ($\text{H}\cdot$) and hydrogen gas (H_2) at the surface of Pd. The H_2 gas is then absorbed onto the Pd NPs and thus partially dissociated back to atomic hydrogen radicals (Equation (3)), which acts as the primary reactive species for hydro-dechlorination. It is noted that the remaining H_2 from the zero-valent Ni NPs synthesis process can also undertake the same processes and dechlorinate 1,2-DCB. When 1,2-DCB adsorbs onto the Pd surface, the cleavage of R-Cl bonds occurs via hydro-dechlorination (Equations (4) and (5)). Figure 4 shows the dechlorination mechanism of 1,2-DCB in the Ni/Pd bimetallic system. According to the results from prior studies, benzene is the ultimate 1,2-DCB dechlorination product [46,47]. Figure 5 shows the plot of degradation ratio of 1,2-DCB and the formation of chlorobenzene and benzene versus the reaction time for the dechlorination reaction of 1,2-DCB with the sample of 24.29 wt.% of Pd loading onto Ni NPs (for the GC chromatograms, see Figure S3) [2,39,40,48–50].

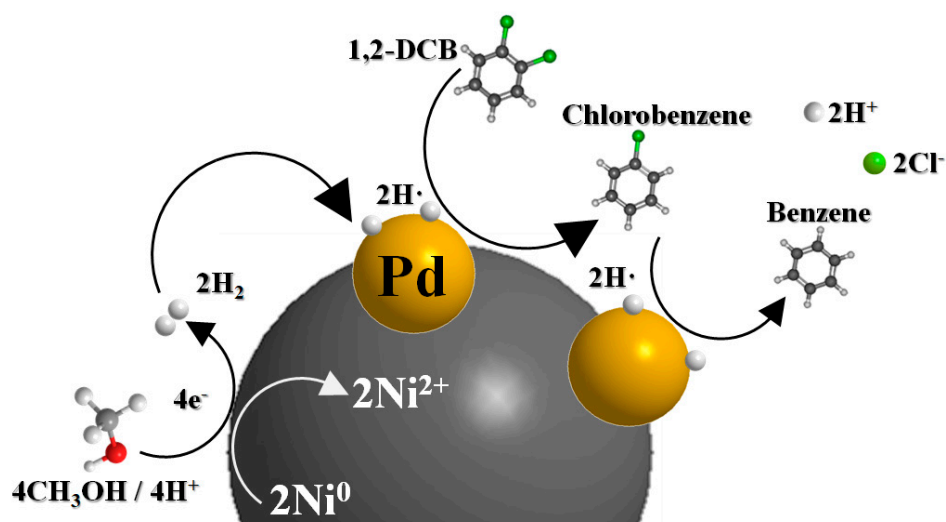


Figure 4. Schematic diagram of catalytic 1,2-DCB dechlorination on the surface of Ni/Pd bimetallic NPs.

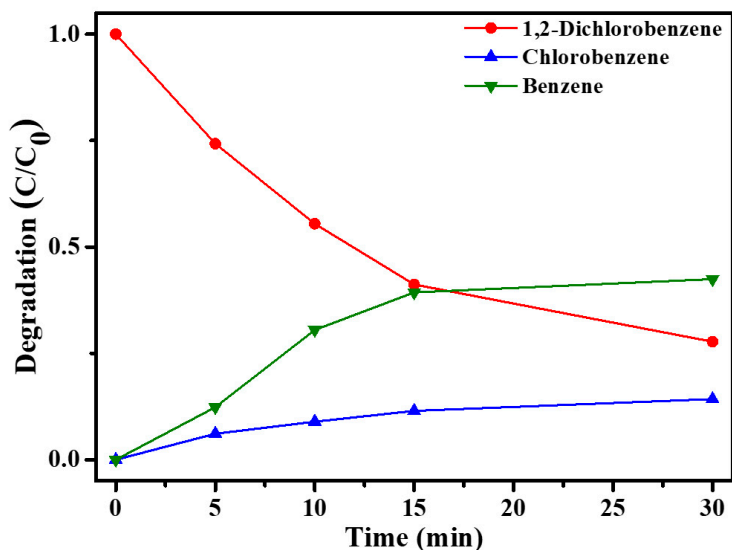


Figure 5. Plot of degradation ratio of 1,2-DCB (●) and formation of chlorobenzene (▲) and benzene (▼) versus the reaction time for the dechlorination reaction of 1,2-DCB with the sample of 24.29 wt.% of Pd loading onto Ni NPs.

3. Materials and Methods

3.1. Chemicals

Nickel plate ($\geq 99.98\%$), palladium(II) chloride (PdCl_2 , 99.99%), and 1,2-DCB ($\text{C}_6\text{H}_4\text{Cl}_2$, 99%) were purchased from Sigma-Aldrich Co., Ltd. (St. Louis, MO, USA). Methanol (99.5%) was purchased from Daejung Co., Ltd. (Busan, Korea). All of the chemicals were used directly without further purification.

3.2. PLAL Conditions

Illustrative experimental outlines are well described elsewhere [34]. In brief, the Ni plate was placed in a 20 mL Pyrex vial of vigorously stirred solvent (10 mL). A LabVIEW program (8.5, National Instruments, Austin, TX, USA) was used to move the Ni plate continuously to provide a fresh sample for the laser ablation. A typical PLAL sequence involves the use of a 30 mm focal lens to focus a pulsed laser onto the Ni plate (~ 1 mm spot). The laser ablation lasted for 20 min with a laser pulse energy of 80 mJ/pulse.

3.3. Preparation of Ni/Pd Bimetallic NPs

Monometallic Pd NPs were synthesized by mixing the PdCl_2 stock solution, prepared by dissolving PdCl_2 in methanol with 0.01 M ascorbic acid (as a reductant) solution, into the Ni colloidal solution with constant stirring at room temperature. Pd/Ni bimetallic NPs were fabricated by mixing the PdCl_2 stock solution into the Ni colloidal solution prepared by PLAL without the reductant [51,52]. When the PdCl_2 stock solution was added to the Ni colloidal solution, the color of the sample changed from dark brown to black, indicating the formation of Pd NPs. The Pd^{2+} ions were easily reduced without a reductant by the electrons that were produced in the PLAL process of synthesizing the Ni NPs in methanol, which have been revealed by the previous studies [53]. The Ni powder/Pd NPs and Ni/Pd bimetallic NPs were synthesized by mixing the PdCl_2 stock solution to the prepared Ni powder and Ni NP solution with constant stirring and sonication for 30 min. The prepared Ni powder/Pd NPs and Ni/Pd bimetallic NPs solution was washed with methanol, and the residues were centrifuged at a rate of 13,000 rpm for 10 min. Different amounts of PdCl_2 (0.51×10^{-4} M (1.60 wt.%), 1.53×10^{-4} M (6.19 wt.%), 2.56×10^{-4} M (19.16 wt.%), and 4.10×10^{-4} M (24.29 wt.%)) were mixed to the solution of Ni powder and Ni NPs and sonicated for 30 min to produce the Ni powder/Pd NPs and Ni/Pd bimetallic NPs.

3.4. Dechlorination of 1,2-DCB

All of the dechlorination experiments were performed with the sediments as catalysts (0.5 mg) and 1.6 mL of 1,2-DCB solution (1.0×10^{-5} M) in methanol. The solutions were ultra-sonicated for 120 min in an ultrasonic water bath (38 kHz at 15-min intervals for each GC experiment). At 15-min intervals, 150 μL of the dechlorinated solution was mixed with 300 μL of hexane in an e-tube and centrifuged (13,000 rpm for 10 min). A 200 μL aliquot was removed from the e-tube and analyzed using gas chromatography.

3.5. Characterization

XRD (AXS D8 Discover with GADDS, Bruker, Billerica, MA, USA) with Cu $\text{K}\alpha$ radiation ($\lambda = 0.15418$ nm), FE-SEM (XL30S FEG, Philips, Amsterdam, Netherlands), HRTEM (TF30ST, Fei-Tecna, Hillsboro, OR, USA), energy dispersive X-ray spectroscopy (EDS; Oxford, UK) with Mn $\text{K}\alpha$ radiation ($\lambda = 138$ eV), and FFT analysis (Gatan, Inc., Pleasanton, CA, USA) were used for the characterization of the as-prepared samples. A gas chromatography (GC-TCD; Master GC, DANI Instruments, Milano, Italy) equipped with a flame ionization detector and a capillary column (HP-5 capillary column, 30 m \times 320 μm \times 0.25 μm) was used for the degradation studies.

4. Conclusions

In summary, we have presented a nanoscale Ni/Pd bimetallic complex by using the facile PLAL technique. The resulting NPs were efficient catalysts for the dechlorination reaction of COCs. The synthesized Ni, Pd, Ni powder/Pd, and Ni/Pd NPs were investigated for the degradation of 1,2-DCB. Among these, Ni/Pd bimetallic NPs showed the maximum degradation rate for 1,2-DCB. The surface chemistry of Ni/Pd bimetallic NPs was directly responsible for the degradation of 1,2-DCB. Furthermore, the optimum Pd loading onto Ni was found to be 19.16 wt.% (100% dechlorination efficiency after 30 min). The fast catalytic activity was attributed to the well-dispersed nature of Pd onto the Ni surface. The rapid dechlorination of 1,2-DCB suggests that the Ni/Pd bimetallic NPs can be used in the purification treatment of polychlorinated aromatic compounds in the environment.

Supplementary Materials: The following are available online at <http://www.mdpi.com/2073-4344/8/9/390/s1>, Figure S1: (i) HRTEM, (ii) enlarged image, and (iii) SAED patterns of pure Ni NPs. (iv) FE-SEM images of (iv) pure Ni NPs, (v) Ni powder, and (vi) Ni powder/Pd NPs, Figure S2: Plot of $\ln(C_t/C_0)$ versus reaction time for the dechlorination reaction of 1,2-DCB by various wt.% of Pd loading onto Ni NPs (■: 1.60 wt.%, ●: 6.19 wt.%, ▲: 19.16 wt.%, ▼: 24.29 wt.%), Figure S3: GC chromatograms of 1,2-DCB with the sample of 24.29 wt.% of Pd loading onto Ni NPs at different reaction time (0, 5, 10, 15, and 30 min).

Author Contributions: Data curation & Formal analysis, H.J.J. and S.J.L.; Writing—original draft, H.J.J. & R.K.; Funding acquisition, S.K.K. and M.Y.C.; Supervision, H.C.C. and M.Y.C.; Writing—review & editing, M.Y.C.

Funding: This research was funded by Basic Science Research Program through the National Research Foundation of Korea (NRF) grant number 2016R1D1A1B03934376 (Ministry of Education) and 2017M2B2A9A02049940, 2017R1A41014595 (S.K. Kim) (Korea government).

Acknowledgments: H. J. Jung acknowledges the travel grant for collaboration on this research supported by Korean Advanced Institute of Women in Science, Engineering and Technology Support Programs for R&D Activities, 2018.

Conflicts of Interest: The authors declare no conflict of interest.

References

1. Gui, M.; Ormsbee, L.E.; Bhattacharyya, D. Reactive functionalized membranes for polychlorinated biphenyl degradation. *Ind. Eng. Chem. Res.* **2013**, *52*, 10430–10440. [[CrossRef](#)] [[PubMed](#)]
2. Xu, F.; Deng, S.; Xu, J.; Zhang, W.; Wu, M.; Wang, B.; Huang, J.; Yu, G. Highly active and stable Ni-Fe bimetal prepared by ball milling for catalytic hydrodechlorination of 4-chlorophenol. *Environ. Sci. Technol.* **2012**, *46*, 4576–4582. [[CrossRef](#)] [[PubMed](#)]
3. Maire, J.; Joubert, A.; Kaifas, D.; Invernizzi, T.; Marduel, J.; Colombano, S.; Cazaux, D.; Marion, C.; Klein, P.Y.; Dumestre, A.; et al. Assessment of flushing methods for the removal of heavy chlorinated compounds DNAPL in an alluvial aquifer. *Sci. Total Environ.* **2018**, *612*, 1149–1158. [[CrossRef](#)] [[PubMed](#)]
4. Yang, P.; Zuo, S.; Zhou, R. Synergistic catalytic effect of $(\text{Ce,Cr})_x\text{O}_2$ and HZSM-5 for elimination of chlorinated organic pollutants. *Chem. Eng. J.* **2017**, *323*, 160–170. [[CrossRef](#)]
5. Jalil, A.A.; Triwahyono, S.; Razali, N.A.M.; Hairom, N.H.H.; Idris, A.; Muhid, M.N.M.; Ismail, A.; Yahaya, N.A.M.; Ahmad, N.A.L.; Dzinun, H. Complete electrochemical dechlorination of chlorobenzenes in the presence of various arene mediators. *J. Hazard. Mater.* **2010**, *174*, 581–585. [[CrossRef](#)] [[PubMed](#)]
6. Cano, M.; Guarín, F.; Aristizábal, B.; Villa, A.L.; González, L.M. Catalytic activity and stability of Pd/Co catalysts in simultaneous selective catalytic reduction of NO_x with methane and oxidation of o-dichlorobenzene. *Catal. Today* **2017**, *296*, 105–117. [[CrossRef](#)]
7. Hosseinkhani, B.; Nuzzo, A.; Zanaroli, G.; Fava, F.; Boon, N. Assessment of catalytic dechlorination activity of suspended and immobilized bio-Pd NPs in different marine conditions. *Appl. Catal. B* **2015**, *168*–169, 62–67. [[CrossRef](#)]
8. Kim, N.R.; Shin, K.; Jung, I.; Shim, M.; Lee, H.M. Ag-Cu Bimetallic Nanoparticles with Enhanced Resistance to Oxidation: A Combined Experimental and Theoretical Study. *J. Phys. Chem. C* **2014**, *118*, 26324–26331. [[CrossRef](#)]
9. Dutta, S.; Ray, C.; Sarkar, S.; Roy, A.; Sahoo, R.; Pal, T. Facile Synthesis of Bimetallic Au-Pt, Pd-Pt, and Au-Pd Nanostructures: Enhanced Catalytic Performance of Pd-Pt Analogue towards Fuel Cell Application and Electrochemical Sensing. *Electrochim. Acta* **2015**, *180*, 1075–1084. [[CrossRef](#)]

10. Chang, L.; Li, Y. One-step encapsulation of Pt-Co bimetallic nanoparticles within MOFs for advanced room temperature nanocatalysis. *Mol. Catal.* **2017**, *433*, 77–83. [[CrossRef](#)]
11. Dong, H.; Jiang, Z.; Deng, J.; Zhang, C.; Cheng, Y.; Hou, K.; Zhang, L.; Tang, L.; Zeng, G. Physicochemical transformation of Fe/Ni bimetallic nanoparticles during aging in simulated groundwater and the consequent effect on contaminant removal. *Water Res.* **2018**, *129*, 51–57. [[CrossRef](#)] [[PubMed](#)]
12. Gołabiewska, A.; Lisowski, W.; Jarek, M.; Nowaczyk, G.; Michalska, M.; Jurga, S.; Zaleska-Medynska, A. The effect of metals content on the photocatalytic activity of TiO₂ modified by Pt/Au bimetallic nanoparticles prepared by sol-gel method. *Mol. Catal.* **2017**, *442*, 154–163. [[CrossRef](#)]
13. Kannan, P.; Yoon, C.S.; Yi, S.C.; Lee, S.Y.; Kim, D.H. Shape-controlled synthesis of gold-nickel bimetallic nanoparticles and their electrocatalytic properties. *Mater. Chem. Phys.* **2015**, *156*, 1–8. [[CrossRef](#)]
14. Lin, J.; Chen, J.; Su, W. Rhodium-cobalt bimetallic nanoparticles: A catalyst for selective hydrogenation of unsaturated carbon-carbon bonds with hydrous hydrazine. *Adv. Synth. Catal.* **2013**, *355*, 41–46. [[CrossRef](#)]
15. Zhang, X.; Wu, D.; Cheng, D. Component-dependent electrocatalytic activity of PdCu bimetallic nanoparticles for hydrogen evolution reaction. *Electrochim. Acta* **2017**, *246*, 572–579.
16. Chen, S.S.; Yang, Z.Z.; Wang, A.J.; Fang, K.M.; Feng, J.J. Facile synthesis of bimetallic gold-palladium nanocrystals as effective and durable advanced catalysts for improved electrocatalytic performances of ethylene glycol and glycerol oxidation. *J. Colloid Interface Sci.* **2018**, *509*, 10–17. [[CrossRef](#)] [[PubMed](#)]
17. Pino, N.; Sitthisa, S.; Tan, Q.; Souza, T.; López, D.; Resasco, D.E. Structure, activity, and selectivity of bimetallic Pd-Fe/SiO₂ and Pd-Fe/γ-Al₂O₃ catalysts for the conversion of furfural. *J. Catal.* **2017**, *350*, 30–40. [[CrossRef](#)]
18. Tuo, Y.; Liu, G.; Dong, B.; Zhou, J.; Wang, A.; Wang, J.; Jin, R.; Lv, H.; Dou, Z.; Huang, W. Microbial synthesis of Pd/Fe₃O₄, Au/Fe₃O₄ and PdAu/Fe₃O₄ nanocomposites for catalytic reduction of nitroaromatic compounds. *Sci. Rep.* **2015**, *5*, 13515. [[CrossRef](#)] [[PubMed](#)]
19. Bedia, J.; Arevalo-Bastante, A.; Grau, J.M.; Dosso, L.A.; Rodriguez, J.J.; Mayoral, A.; Diaz, I.; Gómez-Sainero, L.M. Effect of the Pt-Pd molar ratio in bimetallic catalysts supported on sulfated zirconia on the gas-phase hydrodechlorination of chloromethanes. *J. Catal.* **2017**, *352*, 562–571. [[CrossRef](#)]
20. Fang, D.; Li, W.; Zhao, J.; Liu, S.; Ma, X.; Xu, J.; Xia, C. Catalytic hydrodechlorination of 4-chlorophenol over a series of Pd-Cu/γ-Al₂O₃ bimetallic catalysts. *RSC Adv.* **2014**, *4*, 59204–59210. [[CrossRef](#)]
21. Karanjit, S.; Jinasan, A.; Samsook, E.; Dhital, R.N.; Motomiya, K.; Sato, Y.; Tohji, K.; Sakurai, H. Significant stabilization of palladium by gold in the bimetallic nanocatalyst leading to an enhanced activity in the hydrodechlorination of aryl chlorides. *Chem. Commun.* **2015**, *51*, 12724–12727. [[CrossRef](#)] [[PubMed](#)]
22. Xu, J.; Liu, X.; Lowry, G.V.; Cao, Z.; Zhao, H.; Zhou, J.L.; Xu, X. Dechlorination Mechanism of 2,4-Dichlorophenol by Magnetic MWCNTs Supported Pd/Fe Nanohybrids: Rapid Adsorption, Gradual Dechlorination, and Desorption of Phenol. *ACS Appl. Mater. Interfaces* **2016**, *8*, 7333–7342. [[CrossRef](#)] [[PubMed](#)]
23. Danish, M.; Gu, X.; Lu, S.; Ahmad, A.; Naqvi, M.; Farooq, U.; Zhang, X.; Fu, X.; Miao, Z.; Xue, Y. Efficient transformation of trichloroethylene activated through sodium percarbonate using heterogeneous zeolite supported nano zero valent iron-copper bimetallic composite. *Chem. Eng. J.* **2017**, *308*, 396–407. [[CrossRef](#)]
24. Danish, M.; Gu, X.; Lu, S.; Farooq, U.; Zaman, W.Q.; Fu, X.; Miao, Z.; Brusseau, M.L.; Ahmad, A.; Naqvi, M. An efficient catalytic degradation of trichloroethene in a percarbonate system catalyzed by ultra-fine heterogeneous zeolite supported zero valent iron-nickel bimetallic composite. *Appl. Phys. A* **2017**, *531*, 177–186. [[CrossRef](#)] [[PubMed](#)]
25. Mallikarjuna, K.; Kim, H. Synthesis and characterization of highly active Cu/Pd bimetallic nanostructures. *Colloids Surf. A Physicochem. Eng. Asp.* **2017**, *535*, 194–200. [[CrossRef](#)]
26. Zhao, D.; Li, M.; Zhang, D.; Baig, S.A.; Xu, X. Reductive dechlorination of 2,4-dichlorophenol by Pd/Fe nanoparticles prepared in the presence of ultrasonic irradiation. *Ultrason. Sonochem.* **2013**, *20*, 864–871. [[CrossRef](#)] [[PubMed](#)]
27. Wu, H.; Feng, Q. Fabrication of bimetallic Ag/Fe immobilized on modified biochar for removal of carbon tetrachloride. *J. Environ. Sci.* **2017**, *54*, 346–357. [[CrossRef](#)] [[PubMed](#)]
28. Wu, H.; Feng, Q.; Yang, H.; Alam, E.; Gao, B.; Gu, D. Modified biochar supported Ag/Fe nanoparticles used for removal of cephalixin in solution: Characterization, kinetics and mechanisms. *Colloids Surf. A Physicochem. Eng. Asp.* **2017**, *517*, 63–71. [[CrossRef](#)]

29. Grabowska, E.; Marchelek, M.; Klimczuk, T.; Lisowski, W.; Zaleska-Medynska, A. Preparation, characterization and photocatalytic activity of TiO₂ microspheres decorated by bimetallic nanoparticles. *J. Mol. Catal. A Chem.* **2016**, *424*, 241–253. [[CrossRef](#)]
30. Peng, Z.; Yu, Z.; Wang, L.; Hou, Y.; Shi, Y.; Wu, L.; Li, Z. Facile synthesis of Pd-Fe nanoparticles modified Ni foam electrode and its behaviors in electrochemical reduction of tetrabromobisphenol A. *Mater. Lett.* **2016**, *166*, 300–303. [[CrossRef](#)]
31. Qin, N.; Zhang, Y.; Zhou, H.; Geng, Z.; Liu, G.; Zhang, Y.; Zhao, H.; Wang, G. Enhanced removal of trace Cr(VI) from neutral and alkaline aqueous solution by FeCo bimetallic nanoparticles. *J. Colloid Interface Sci.* **2016**, *472*, 8–15. [[CrossRef](#)] [[PubMed](#)]
32. Wang, X.; Liu, C.; Chen, H.; Ma, J. Characterization and evaluation of catalytic dechlorination activity of Pd/Fe bimetallic nanoparticles. *Ind. Eng. Chem. Res.* **2008**, *47*, 8645–8651. [[CrossRef](#)]
33. Amendola, V.; Scaramuzza, S.; Carraro, F.; Cattaruzza, E. Formation of alloy nanoparticles by laser ablation of Au/Fe multilayer films in liquid environment. *J. Colloid Interface Sci.* **2017**, *489*, 18–27. [[CrossRef](#)] [[PubMed](#)]
34. Jung, H.J.; Choi, M.Y. Specific Solvent Produces Specific Phase Ni Nanoparticles: A Pulsed Laser Ablation in Solvents. *J. Phys. Chem. C* **2014**, *118*, 14647–14654. [[CrossRef](#)]
35. Sivasakthi, P.; Ramesh Babu, G.N.K.; Chandrasekaran, M.; Sreejakumari, S.S. Synthesis of a super-hydrophobic Ni-ITO nanocomposite with pine-cone and spherical shaped micro-nanoarchitectures by pulse electrodeposition and its electrocatalytic application. *RSC Adv.* **2016**, *6*, 44766–44773. [[CrossRef](#)]
36. Sengupta, D.; Saha, J.; De, G.; Basu, B. Pd/Cu bimetallic nanoparticles embedded in macroporous ion-exchange resins: An excellent heterogeneous catalyst for the Sonogashira reaction. *J. Mater. Chem. A* **2014**, *2*, 3986–3992. [[CrossRef](#)]
37. Bhattacharjee, D.; Dasgupta, S. Trimetallic NiFePd nanoalloy catalysed hydrogen generation from alkaline hydrous hydrazine and sodium borohydride at room temperature. *J. Mater. Chem. A* **2015**, *3*, 24371–24378. [[CrossRef](#)]
38. Maity, M.; Maitra, U. An easily prepared palladium-hydrogel nanocomposite catalyst for C-C coupling reactions. *J. Mater. Chem. A* **2014**, *2*, 18952–18958. [[CrossRef](#)]
39. Zhou, T.; Li, Y.; Lim, T.T. Catalytic hydrodechlorination of chlorophenols by Pd/Fe nanoparticles: Comparisons with other bimetallic systems, kinetics and mechanism. *Sep. Purif. Technol.* **2010**, *76*, 206–214. [[CrossRef](#)]
40. Nagpal, V.; Bokare, A.D.; Chikate, R.C.; Rode, C.V.; Paknikar, K.M. Reductive dechlorination of γ -hexachlorocyclohexane using Fe-Pd bimetallic nanoparticles. *J. Hazard. Mater.* **2010**, *175*, 680–687. [[CrossRef](#)] [[PubMed](#)]
41. Yu, Y.; Jung, H.J.; Je, M.; Choi, H.C.; Choi, M.Y. Enhanced dechlorination of m-DCB using iron-graphite/palladium (Fe-C/Pd) nanoparticles produced by pulsed laser ablation in liquid. *Chemosphere* **2016**, *155*, 250–256. [[CrossRef](#)] [[PubMed](#)]
42. Zhou, J.; Chen, H.; Chen, Q.; Huang, Z. Bimetallic Au-decorated Pd catalyst for the liquid phase hydrodechlorination of 2,4-dichlorophenol. *Appl. Surf. Sci.* **2016**, *387*, 588–594. [[CrossRef](#)]
43. Seshu Babu, N.; Lingaiah, N.; Sai Prasad, P.S. Characterization and reactivity of Al₂O₃ supported Pd-Ni bimetallic catalysts for hydrodechlorination of chlorobenzene. *Appl. Catal. B* **2012**, *111–112*, 309–316. [[CrossRef](#)]
44. Kim, P.; Kim, Y.; Kim, H.; Song, I.K.; Yi, J. Preparation, characterization, and catalytic activity of NiMg catalysts supported on mesoporous alumina for hydrodechlorination of o-dichlorobenzene. *J. Mol. Catal. A Chem.* **2005**, *231*, 247–254. [[CrossRef](#)]
45. Schrick, B.; Blough, J.L.; Jones, A.D.; Mallouk, T.E. Hydrodechlorination of trichloroethylene to hydrocarbons using bimetallic nickel-iron nanoparticles. *Chem. Mater.* **2002**, *14*, 5140–5147. [[CrossRef](#)]
46. Han, Y.; Liu, C.; Horita, J.; Yan, W. Trichloroethene hydrodechlorination by Pd-Fe bimetallic nanoparticles: Solute-induced catalyst deactivation analyzed by carbon isotope fractionation. *Appl. Catal. B* **2016**, *188*, 77–86. [[CrossRef](#)]
47. Shen, W.; Mu, Y.; Wang, B.; Ai, Z.; Zhang, L. Enhanced aerobic degradation of 4-chlorophenol with iron-nickel nanoparticles. *Appl. Surf. Sci.* **2017**, *393*, 316–324. [[CrossRef](#)]
48. Xu, J.; Lv, X.; Li, J.; Li, Y.; Shen, L.; Zhou, H.; Xu, X. Simultaneous adsorption and dechlorination of 2,4-dichlorophenol by Pd/Fe nanoparticles with multi-walled carbon nanotube support. *J. Hazard. Mater.* **2012**, *225–226*, 36–45. [[CrossRef](#)] [[PubMed](#)]

49. Lin, C.J.; Lo, S.L.; Liou, Y.H. Dechlorination of trichloroethylene in aqueous solution by noble metal-modified iron. *J. Hazard. Mater. B* **2004**, *116*, 219–228. [[CrossRef](#)] [[PubMed](#)]
50. Feng, J.; Lim, T.T. Pathways and kinetics of carbon tetrachloride and chloroform reductions by nano-scale Fe and Fe/Ni particles: Comparison with commercial micro-scale Fe and Zn. *Chemosphere* **2005**, *59*, 1267–1277. [[CrossRef](#)] [[PubMed](#)]
51. Jana, N.R.; Wang, Z.L.; Pal, T. Redox Catalytic Properties of Palladium Nanoparticles: Surfactant and Electron Donor-Acceptor Effects. *Langmuir* **2000**, *16*, 2457–2463. [[CrossRef](#)]
52. Castegnaro, M.V.; Kilian, A.S.; Baibich, I.M.; Alves, M.C.M.; Morais, J. On the Reactivity of Carbon Supported Pd Nanoparticles during NO Reduction: Unraveling a Metal-Support Redox Interaction. *Langmuir* **2013**, *29*, 7125–7133. [[CrossRef](#)] [[PubMed](#)]
53. Lee, S.; Ahn, A.; Choi, M.Y. Direct observation of aluminium ions produced via pulsed laser ablation in liquid: A ‘turn-on’ fluorescence study. *Phys. Chem. Chem. Phys.* **2012**, *14*, 15677–15681. [[CrossRef](#)] [[PubMed](#)]



© 2018 by the authors. Licensee MDPI, Basel, Switzerland. This article is an open access article distributed under the terms and conditions of the Creative Commons Attribution (CC BY) license (<http://creativecommons.org/licenses/by/4.0/>).